Knowledge-Based Systems 227 (2021) 107189

Contents lists available at ScienceDirect

Knowledge-Based Systems

journal homepage: www.elsevier.com/locate/knosys

Global EM-driven optimization of multi-band antennas using knowledge-based inverse response-feature surrogates

Slawomir Koziel [a,b], Anna Pietrenko-Dabrowska [b,*]

[a] Engineering Optimization & Modeling Center, Reykjavik University, 102 Reykjavik, Iceland
[b] Faculty of Electronics, Telecommunications and Informatics, Gdansk University of Technology, 80-233 Gdansk, Poland

ARTICLE INFO

Article history:
Received 6 April 2021
Received in revised form 26 May 2021
Accepted 31 May 2021
Available online 6 June 2021

Keywords:
Antenna design
EM-driven design
Global optimization
Knowledge-based optimization
Data-driven optimization
Response features
Surrogate modelling
Inverse modelling

ABSTRACT

Electromagnetic simulation tools have been playing an increasing role in the design of contemporary antenna structures. The employment of electromagnetic analysis ensures reliability of evaluating antenna characteristics but also incurs considerable computational expenses whenever massive simulations are involved (e.g., parametric optimization, uncertainty quantification). This high cost is the most serious bottleneck of simulation-driven design procedures, and may be troublesome even for local tuning of geometry parameters, let alone global optimization. On the one hand, globalized search is often necessary because the design problem might be multimodal (i.e., the objective function features multiple local optima) or a reasonably good initial design may not be available. On the other hand, the computational efficiency of popular algorithmic approaches, primarily, nature-inspired population-based algorithms, is generally poor. Combining metaheuristics procedures with surrogate modelling techniques and sequential sampling methods alleviates the problem to a certain extent but modelling of nonlinear antenna responses over broad frequency ranges is extremely challenging, and the aforementioned solutions are normally limited to rather simple structures described by a few parameters. This paper proposes a novel approach to global optimization of multi-band antennas. The major component of the presented framework is the knowledge-based inverse surrogate constructed at the level of response features (e.g., frequency and level locations of the antenna resonances). The surrogate facilitates decision-making process of inexpensive identification of the most promising regions of the parameter space, and a rendition of the good-quality initial design for further local tuning. Our methodology is validated using three examples of dual- and triple-band antennas. The average optimization cost is only 150 full-wave antenna analyses while ensuring precise allocation of the antenna resonances at the target frequencies. This performance is demonstrated superior over both local optimizers and population-based metaheuristics.

1. Introduction

Geometrical complexity of antenna systems has been growing considerably over the last decade or so, partially due to increasing performance demands incurred by emerging application areas (5G wireless communications [1,2], wireless sensing [3], microwave imaging [4], internet of things, IoT [5], etc.), but also additional functionalities (MIMO operation [6], tunable antennas [7], enhanced gain [8], pattern diversity [9]). Another reason is miniaturization, essential for mobile communication [10], wearable or implantable devices [11,12]. This fosters the development of unconventional antenna topologies featuring components such as slots [13], stubs [14], defected ground structures [15], shorting pins [16], multi-layer structures [17], etc. Adequate evaluation of geometrically complex antennas requires full-wave electromagnetic (EM) analysis.

One of the consequences of the structural complexity of modern antennas is that EM-driven optimization becomes instrumental in ensuring cutting-edge performance. Neither circuit theory tools nor parametric studies are capable of yielding satisfactory designs. Unfortunately, simulation-based design is often computationally expensive, even if only local parameter tuning is to be executed. Often the need for global search arises [18–24], entailing considerably higher costs [25,26]. Examples include multimodal problems (e.g., optimization of frequency-selective surfaces [27], pattern synthesis of antenna arrays [28,29]), or simply the lack of reasonable initial design [30]. The latter typically occurs when the antenna structure at hand contains a number of topological alterations that implement additional functionalities or facilitate size reduction (e.g., stubs or slots) [31,32].

Nowadays, the most popular methods for global optimization are undoubtedly nature-inspired algorithms [33–41]. Initially

* Corresponding author.
E-mail addresses: koziel@ru.is (S. Koziel), anna.dabrowska@pg.edu.pl (A. Pietrenko-Dabrowska).

https://doi.org/10.1016/j.knosys.2021.107189

conceived in the 1980s (e.g., genetic algorithms [42], evolutionary algorithms [43], ant systems [44], although evolutionary strategies [45] date back to late 1960s), underwent significant developments in 1990s (e.g., particle swarm optimizers, PSO [46], differential evolution [47]), to eventually dominate global optimization practice since early 2000s. Recent years observed a rapid growth in the number of methods (firefly algorithm [48], harmony search [49], grey wolf optimization [50], and others [51–53]). By exchanging information between the members of the population being processed, as well as producing new information using both exploratory and exploitative operators [54], the promising regions of the parameter space can be identified, which enables global search capability. Nature-inspired algorithms are typically straightforward to implement but computationally inefficient (the number of objective function evaluations of even several thousand within a single algorithm run [55,56]). When the antenna under design is evaluated using EM analysis, the associated CPU cost becomes unmanageable.

Therefore, practical applicability of population-based techniques in antenna optimization is limited to cases when the objective function is fast to evaluate (e.g., analytical array factor models in pattern synthesis tasks [57,58]), the EM analysis cost is low, or computational resources (and licencing) enable parallelization. Another possible workaround is the incorporation of surrogate modelling techniques [59–61], such as kriging [62], Gaussian Process Regression (GPR) [63], or neural networks [64]. The surrogate construction is typically interleaved with the search process by incorporating the available high-fidelity data. The allocation of infill samples may be based on various criteria to either aid the parameter space exploration or exploitation [65]. The alternatives include machine learning techniques [66,67], also combined with sequential sampling methods [68]. Another option is pre-screening of the parameter space using auxiliary surrogates or variable-fidelity simulations [69].

In antenna design, utilization of surrogate modelling techniques is severely hindered by the curse of dimensionality as well as highly nonlinear relationships between the geometry parameters and antenna characteristics. Consequently, applicability of surrogate-assisted nature-inspired methods is normally limited to structures described by a small number of parameters within narrow ranges thereof [70–72]. The recently proposed performance-driven modelling techniques [73–75] allow for alleviating the dimensionality issues by restricting the model domain to a region containing the designs that are optimum with respect to the performance figures relevant to the design task at hand [76]. Domain confinement permits a rendition of accurate surrogates over broad ranges of parameters and operating conditions using small number of training data samples [75] (that can be further reduced using variable-fidelity EM simulations [77]). Recently, the performance-driven modelling paradigm has been also applied to speed up multi-objective design procedures [78]. The major component of the aforementioned approaches is a two-step process with the inverse surrogate employed to identify the parameter space region model domain definition purposes, which capitalizes on the slightly-nonlinear relationships between the geometry parameters and the operating conditions of the antenna [75]. Another recent approach applied to reduce the cost of EM-driven modelling and optimization procedures is the response feature technology [79,80]. Therein, the optimization (or modelling) task is reformulated in terms of appropriately defined characteristic points of the antenna outputs (e.g., frequency/level allocation of multi-band antenna resonances), less nonlinearly dependent on antenna geometry parameters than the entire frequency characteristics. This translates into faster convergence of the optimization process [79], or a significant reduction of data acquisition cost in the modelling context [81].

This paper proposes an algorithmic framework for globalized optimization of multi-band antenna structures. Our methodology incorporates the inverse-modelling-based identification of the promising parameter space regions and the response feature technology for extracting the antenna operating parameters from the EM simulation data. Both mechanisms are utilized to render an initial design, further tuned by means of trust-region gradient search procedure. The inverse model is constructed based on pre-selected data obtained through stochastic search. During the selection process relevant knowledge about the antenna operational parameters is extracted from its simulated responses. This knowledge is then utilized to facilitate a decision-making process of cost-efficient identification of the parameter space regions containing high-quality designs. The major novelties and technical contributions of this work include: (i) conceptual development of the knowledge-based decision-making process that allows for identifying the most promising regions of the parameter space, (ii) implementation of the algorithmic framework for global optimization of multi-band antennas using feature-based inverse surrogates, (iii) realization of the cost-efficient rendition of high-quality initial designs using system-specific knowledge, (iv) demonstrating the efficacy of the proposed approach in solving global optimization problems for multi-band antennas at a cost comparable to that of the local search.

The presented framework is validated using three microstrip antennas optimized to allocate their operating frequencies at specific target values and improve matching therein. The results indicate that our algorithm consistently yields satisfactory designs, whereas its computational complexity is comparable to that of local optimization routines. Comprehensive benchmarking demonstrates its superiority over both multiple-run local search and the state-of-the-art nature-inspired algorithms.

2. Global optimization of multi-band antennas by knowledge-based inverse surrogates and response features

This section provides a detailed exposition of the proposed procedure for globalized optimization of multi-band antennas. The major mechanism incorporated into the algorithm is the feature-based inverse surrogate that allows for rendering good initial designs for further (local) parameter tuning. The core routine is generic, yet, in this work, we focus on multi-band antennas because response feature identification is facilitated for such devices by the very structure of their input characteristics. Generalization of the procedure for other classes of antenna systems will be considered elsewhere. The key concept of our approach is to exploit the knowledge about the relationships between the operational parameters (e.g., operating frequencies), and physical dimensions or material parameters of the antenna under design, and to encode it in the form of the inverse surrogate constructed at the level of the response features. This surrogate is then utilized for identifying the most promising regions of the parameter space and finding the high-quality initial design therein.

2.1. Design problem formulation

This work considers global optimization of input characteristics of multi-band antennas. The design task is to allocate the antenna resonances at the target frequencies $f_{0,j}$, $j = 1, \ldots, K$, where K is the number operating bands. Let $S_{11}(\boldsymbol{x}, f)$ denote the EM-simulated antenna reflection response at the frequency f, with $\boldsymbol{x}$ being a vector of designable variables. The task is to solve

$$\boldsymbol{x}^* = \arg\min_{\boldsymbol{x}} U(\boldsymbol{x}, \boldsymbol{f}_t) \quad (1)$$

where U is a scalar merit function to be minimized, whereas $\boldsymbol{f}_t = [f_{t.1} \ldots f_{t.K}]^T$ is a target vector of operating frequencies. The merit function is defined in a minimax sense

$$U(\boldsymbol{x}, \boldsymbol{f}_t) = \max_{\boldsymbol{x}} \{|S_{11}(\boldsymbol{x}, f_{t.1})|, \ldots, |S_{11}(\boldsymbol{x}, f_{t.K})|\} \quad (2)$$

It should be noted that the formulation (1), (2) can be generalized to consider, e.g., matching improvement over bandwidths, as well as to include other antenna characteristics. Here, we focus on the objective function (2) as a representative case study used to explain the proposed globalized search procedure.

2.2. Response features for initial design quality assessment of multi-band antennas

As explained in the introduction, appropriate tuning of geometry parameters is instrumental in achieving satisfactory performance of antenna structures. For reliability reasons, it is normally conducted at the level of EM simulation models. In many cases, it has to be carried out in a global sense, for example, if the problem at hand is multi-modal (i.e., multiple local optimal are present), or a sufficiently good initial design is not available. In practice, both issues may occur at the same time. Common examples include design of compact structures, where the introduction of various topological modifications leads to parameter redundancy, or re-design of multi-band antennas for operating frequencies considerably different from those at the current design. The primary challenge of globalized search is to conduct exploration of the entire parameter space, which is hindered by considerable nonlinearity and variability of antenna characteristics, especially in terms of large shifts of the operating frequencies across the design space. The same reasons make a construction of globally accurate surrogates virtually impossible.

In this work, we focus on multi-band antennas, where the primary objective is to allocate the antenna resonances at the target operating frequencies. If the parameter space is large in terms of the considered parameter ranges, the resonances will be distributed outside the frequency range of simulation or allocated too far away from the target values for the vast majority of randomly picked variable vectors. In either case, local optimization is unable to yield a satisfactory design. This is illustrated in Fig. 1 for an exemplary dual-band dipole antenna.

Despite the aforementioned issues, extracting information about the allocation of antenna resonances (both in terms of their frequency and level coordinates) may be useful to facilitate the global search procedures. Processing of these so-called characteristic points of antenna responses has been a foundation of the feature-based optimization (FBO) technology proposed in [79]. FBO capitalizes on slightly nonlinear dependence between the antenna geometry parameters and the feature point coordinates [81]. An example of such a relationship has been shown in Fig. 2 for the dual-band antenna of Fig. 1.

The feature points can be extracted from the complete antenna characteristics through post-processing. In general, the characteristic point definition depends on the design problem formulation. For the considered dual-band antenna example, if the goal is to allocate its resonances at the given target frequencies and to minimize the reflection level therein, the suitable response features are just the frequency and level coordinates of the resonances. If the objective is to maximize the fractional bandwidth around the target frequencies, a more convenient characteristics points would be the frequencies corresponding to -10 dB reflection level (see, e.g., [79] for a more extensive discussion of the subject). In this work, the feature points corresponding to antenna resonances will be used for design quality assessment in the first stage of the proposed global search algorithm (cf. Section 2.4).

2.3. Global search using inverse surrogates

As mentioned in Section 2.2, extracting and processing characteristic points of the antenna responses is a powerful tool for evaluating the design quality, especially in terms of the misalignment between the actual and target operating frequencies. In this work, we exploit the weakly nonlinear relationships between the operating frequencies and geometry parameters as illustrated in Fig. 2 for the dual-band antenna example. At this point, it should be mentioned that a similar concept was a foundation of performance-driven modelling frameworks [76].

Therein, the domain of the surrogate was established by approximating the optimum design manifold using an auxiliary inverse model constructed using a set of reference designs optimized for selected vectors of target operating conditions (e.g., operating frequencies in the case of multi-band antennas). This allowed for restricting the volume of the domain and a rendition of accurate surrogates using very limited number of training data samples [75]. In [75], the inverse model was constructed using kriging interpolation [59]. The employment of interpolative models was justified by the fact that the reference points were allocated on the aforementioned optimum design manifold. This is clearly convenient but not directly applicable in this work, because pre-optimized designs are not available in a global optimization context.

The approach developed in this work is loosely related to performance-driven modelling concepts yet is does not assume the availability of any pre-optimized points. Instead, it only uses a set of random observables generated over the antenna parameter space, which may or may not be of good quality. The quality assessment is realized using the problem-specific knowledge in the form of characteristic points of antenna reflection characteristics outlined in Section 2.2. Selected observables are used for construction of a regression-based inverse surrogate, which is subsequently employed to generate the infill points in the most promising regions of the parameter space. The decision-making procedure is iterated until a sufficiently good initial design is found for further local tuning. In each iteration, the current set of observables is refined by replacing the worst designs by those that are of higher quality with respect to the assumed design objectives. The remaining part of this sub-section provides a general outline of the method, followed by a detailed pseudocode.

The following notation will be used throughout:

- $\boldsymbol{F}(\boldsymbol{x}) = [f_1(\boldsymbol{x}) \ldots f_K(\boldsymbol{x})]^T$ – a vector of antenna operating frequencies at the design $\mathbf{x}$ (i.e., frequency coordinates of the feature points); if, for any reason (e.g., some of the antenna resonances are allocated outside the EM simulation frequency range) some of f_ks cannot be extracted, a zero vector $\boldsymbol{F}(\boldsymbol{x}) = [0 \ldots 0]^T$ is assigned;
- $\boldsymbol{L}(\boldsymbol{x}) = [l_1(\boldsymbol{x}) \ldots l_K(\boldsymbol{x})]^T$ – a vector of antenna reflection levels at the operating frequencies at the design $\mathbf{x}$ (i.e., level coordinates of the feature points); if, for any reason some of f_ks cannot be extracted, a zero vector $\boldsymbol{L}(\boldsymbol{x}) = [0 \ldots 0]^T$ is assigned;
- $D(\boldsymbol{F}, \boldsymbol{f}_t)$ – a distance function determining the misalignment between the target vector of operating frequencies $\boldsymbol{f}_t$ (cf. Section 2.1) and a given operating frequency vector $\boldsymbol{F}$; a simple example is an Euclidean norm $D(\boldsymbol{F}, \boldsymbol{f}_t) = \| \boldsymbol{F} - \boldsymbol{f}_t \|$, but in this work we use the infinity norm, i.e., $D(\boldsymbol{F}, \boldsymbol{f}_t) = \| \boldsymbol{F} - \boldsymbol{f}_t \|_\infty$ to account for the worst-case scenario;
- D_{accept} – user-defined threshold distance to determine whether the best design obtained so far with the corresponding operating frequency vector $\boldsymbol{F}$ is sufficiently close to the target, i.e., if $D(\boldsymbol{F}, \boldsymbol{f}_t) \leq D_{accept}$;

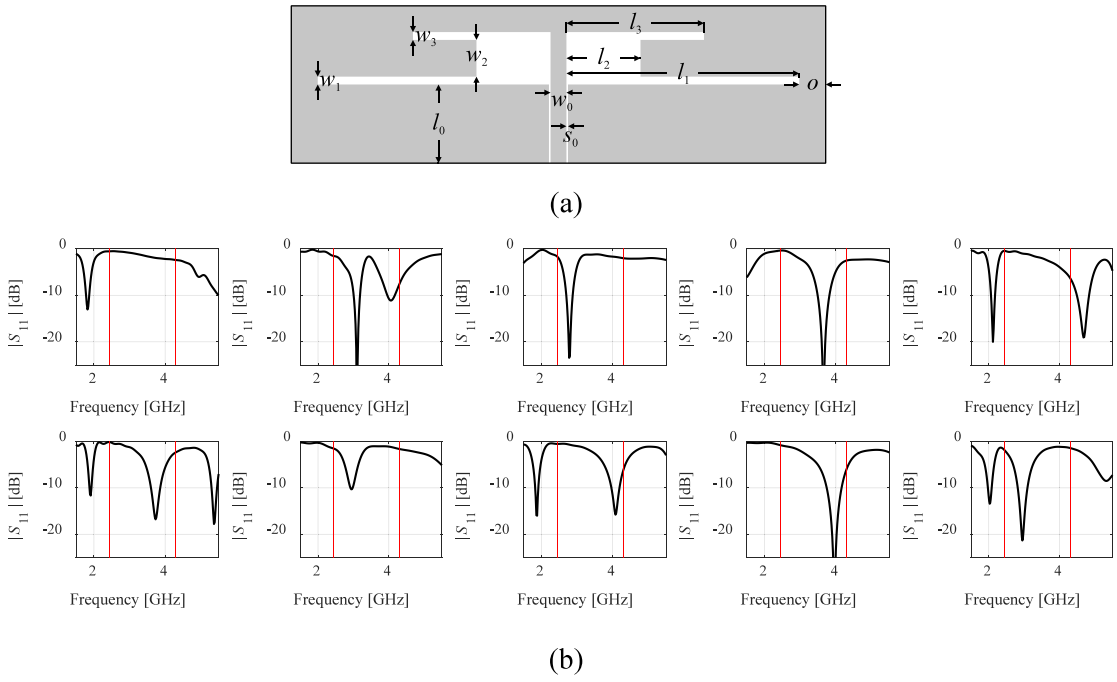

Fig. 1. Exemplary dual-band antenna and its reflection characteristics: (a) antenna geometry, (b) reflection responses at selected designs randomly assigned within the assumed parameter space. The vertical lines mark the target operating frequencies (here, 2.45 GHz and 4.3 GHz). Initiating the local search, e.g., in the minimax sense of reducing the reflection level at and around the target frequencies, from the majority of the shown designs would lead to a failure due to poor initial allocation of the antenna resonances.

The global search procedure employs the following steps (a rigorous description is provided later on):

1. Generate a set of random vectors $\boldsymbol{x}^{(j)}$, $j = 1, \ldots, N$, over the assumed parameter space X (typically, determined by the lower and upper bounds for design variables), such that $\|\boldsymbol{F}(\boldsymbol{x}^{(j)})\| > 0$ for all j. The set is found by sequentially generating random observables until N vectors satisfying the above condition have been found.
2. Construct an inverse regression model $r_I(\boldsymbol{F})$ with the values in X, that represents the relationship between the antenna operating frequencies and geometry parameters; the model is established using the feature vectors $\boldsymbol{F}(\boldsymbol{x}^{(j)})$ and $\boldsymbol{L}(\boldsymbol{x}^{(j)})$, as well as the corresponding parameter vectors $\boldsymbol{x}^{(j)}$.
3. Use r_I as a predictor to find a candidate design $\boldsymbol{x}_{tmp} = r_I(\boldsymbol{f}_t)$, where $\boldsymbol{f}_t$ is the vector of target operating frequencies (cf. Section 2.1). If $\|\boldsymbol{F}(\boldsymbol{x}_{tmp})\| > 0$ and $D(\boldsymbol{F}(\boldsymbol{x}_{tmp}), \boldsymbol{f}_t) < \max\{j = 1, \ldots, N : D(\boldsymbol{F}(\boldsymbol{x}^{(j)}), \boldsymbol{f}_t)\}$, replace the vector ensuring the above maximum by $\boldsymbol{x}_{tmp}$;

The steps 2 and 3 are iterated until identifying the candidate satisfying $D(\boldsymbol{F}(\boldsymbol{x}_{tmp}), \boldsymbol{f}_t) < D_{\max}$ (a user-defined acceptance threshold), upon which the local refinement is executed as described in Section 2.4. In plain words, the procedure generates random observables until a sufficient number of designs have been found for which clearly defined feature points (here, antenna resonances) can be extracted. Subsequently, the inverse model (similar to what has been visualized in Fig. 2(b)) is constructed and used to predict a location of the design for which the operating frequencies are possibly close to the target $\boldsymbol{f}_t$. This design replaces one of the base designs $\boldsymbol{x}^{(j)}$ assuming it is of sufficient quality in terms of the metric $D(\boldsymbol{F}, \boldsymbol{f}_t)$. Over the iterations, the inverse model will be gradually more and more focused in the vicinity of the parameter space region that contains the designs featuring low values of $D(\boldsymbol{F}, \boldsymbol{f}_t)$. Concentration of these base designs would also lead to the improved local accuracy of the inverse model. Fig. 3 shows a graphical explanation of the procedure.

As mentioned above, the critical component of the procedure is the inverse model $r_I(\boldsymbol{F})$ established using the feature vectors $\boldsymbol{F}(\boldsymbol{x}^{(j)})$ and $\boldsymbol{L}(\boldsymbol{x}^{(j)})$. Due to typically weakly nonlinear dependence between the feature points and geometry parameters, the following analytical form of the model has been assumed:

$$\boldsymbol{r}_I(\boldsymbol{F}) = \boldsymbol{r}_I\left([f_1 \ldots f_K]^T\right) = \begin{bmatrix} r_{I.1}(\boldsymbol{F}) \\ \cdots \\ r_{I.n}(\boldsymbol{F}) \end{bmatrix} = \begin{bmatrix} p_{1.0} + p_{1.1} \exp\left(\sum_{k=1}^{K} p_{1.k+1} f_k\right) \\ \cdots \\ p_{n.0} + p_{n.1} \exp\left(\sum_{k=1}^{K} p_{n.k+1} f_k\right) \end{bmatrix} \tag{3}$$

The model coefficients are obtained by solving the nonlinear regression problems of the form

$$\left[p_{j.0}\ p_{j.1} \ldots p_{j.K+1}\right] = \arg\min_{[b_0 b_1 \ldots b_{K+1}]} \sum_{k=1}^{N} w_k \left[r_{I.j}\left(\boldsymbol{F}(\boldsymbol{x}^{(k)})\right) - x_j^{(k)}\right]^2$$
$$j = 1, \ldots, n \tag{4}$$

where $x_j^{(k)}$ is the jth component of the parameter vector $\boldsymbol{x}^{(j)}$, whereas the weighting factors w_k are related to the level coordinates of the feature points as

$$w_k = \left[1 - \max\{l_1(\boldsymbol{x}^{(j)}), \ldots, l_k(\boldsymbol{x}^{(j)})\}\right]^2 \quad k = 1, \ldots, N \tag{5}$$

In other words, the inverse model is set up as a trend function approximating the observables $\boldsymbol{x}^{(j)}$ in the sense of (2), i.e., weighted L-square.

The weighting factors are introduced to put more emphasis on the points corresponding to deeper resonances, as those designs are closer to the optimum design manifold (cf. [75]). Examples

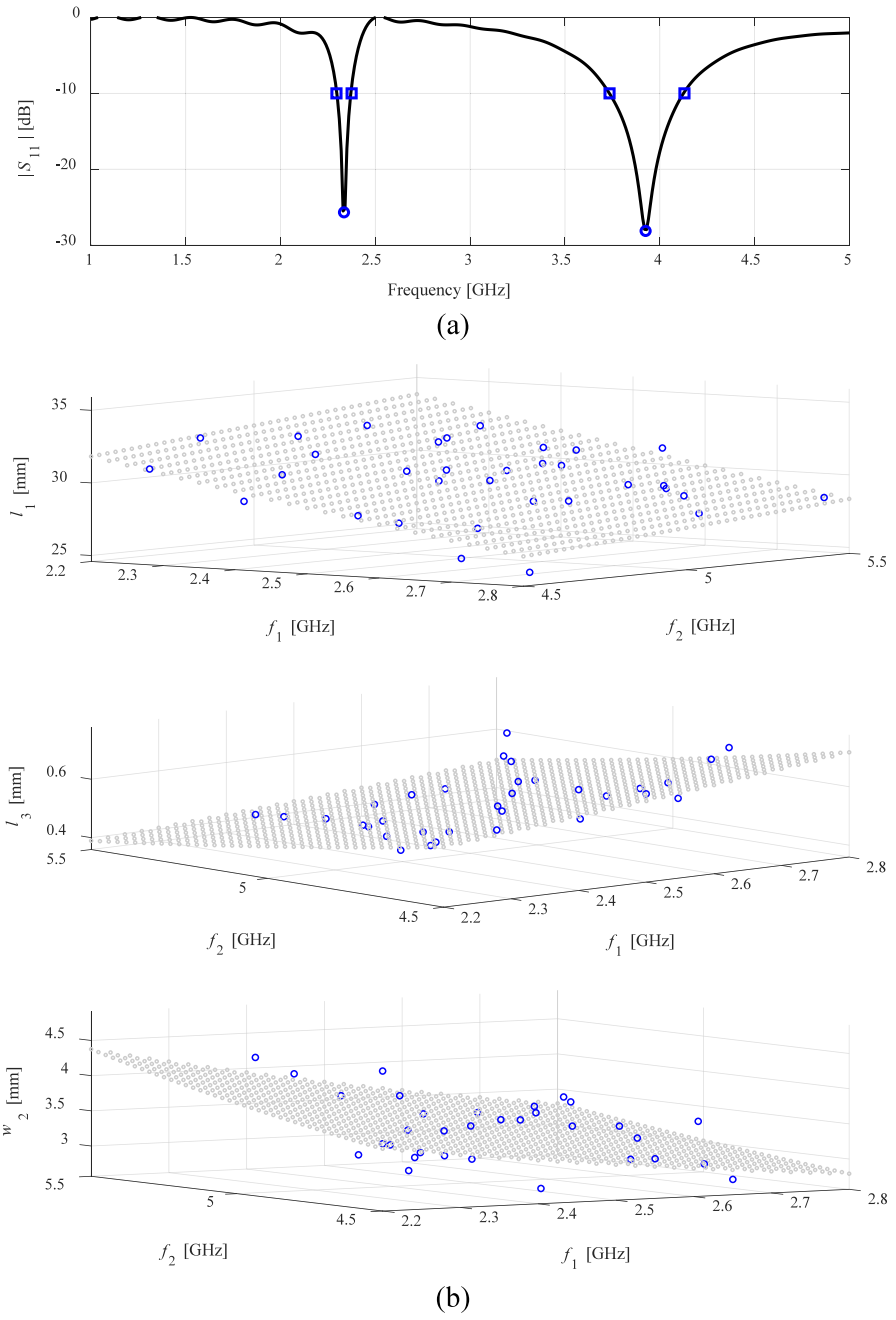

Fig. 2. Dual-band dipole antenna: (a) response features corresponding to antenna resonances (o) and −10 dB reflection levels (□); note that some of the feature points may not exist depending on the design (e.g., one of the resonances being outside the simulation frequency range); (b) relationship between the operating frequencies and the three selected geometry parameters. The circles represent specific antenna designs, whereas the grey points denote the regression model of the form $a_0 + a_1\exp(a_2 f_1 + a_3 f_2)$ representing the trends between the operating frequencies and antenna dimensions. It should be noted that the trends are smooth and weakly nonlinear.

of the surfaces representing the inverse model can be found in Fig. 2(b).

Now we are in a position to provide a rigorous formulation of the global search procedure outline above. It works as follows:

1. Set $j = 1$;
2. Generate a random vector $\boldsymbol{x}^{(j)} \in X$;
3. **if** $\|\boldsymbol{F}(\boldsymbol{x}^{(j)})\| > 0$
   Accept $\boldsymbol{x}(j)$; set $j = j + 1$;
   end
4. **if** $j \leq N$ AND computational budget has not been exceeded
   Go to 2;
   else
   Go to 5;
   end
5. Construct the inverse regression model $r_I(\boldsymbol{F})$ as in (3)–(5);
6. Generate a candidate design $\boldsymbol{x}_{tmp} = r_I(\boldsymbol{f}_t)$, where $\boldsymbol{f}_t$ is the vector of target operating frequencies (cf. Section 2.1);
7. **if** $\|\boldsymbol{F}(\boldsymbol{x}_{tmp})\| > 0$ AND $D(\boldsymbol{F}(\boldsymbol{x}_{tmp}), \boldsymbol{f}_t) < D_{\max} = \max\{j = 1, \ldots, N: D(\boldsymbol{F}(\boldsymbol{x}^{(j)}), \boldsymbol{f}_t)\}$

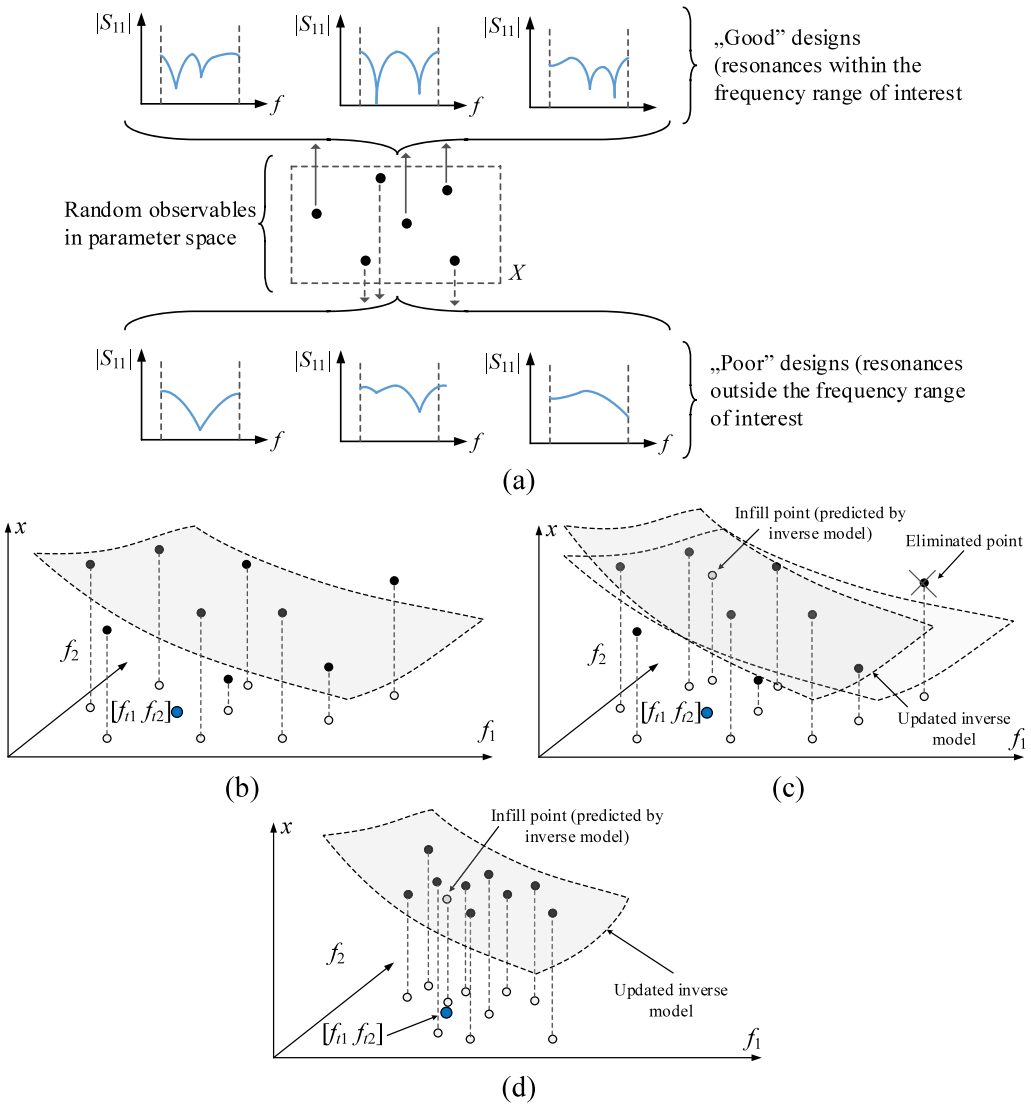

Fig. 3. Graphical illustration of the basic components of the proposed knowledge-based global optimization procedure: (a) generation of random observables: the decision-making process allows for selecting only the parameter vectors for which the corresponding antenna responses have resonances within the simulation frequency range, which are further utilized for inverse model construction, (b) observables (•) in the two-dimensional operating frequency space f_1, f_2 for a selected geometry parameter x along with their projections onto the f_1-f_2 plane, and the initial inverse model (grey surface); target operating frequencies marked using blue circle; (c) first iteration of the global search process: the infill point predicted by the inverse model (marked using grey circle) replaces the worst observable and the inverse model is updated; the procedure is then repeated; (d) last iteration: the observables are concentrated near the target frequencies and the updated inverse model yields the design which is sufficiently close to the target; the procedure is terminated and followed by local refinement (Section 2.4). Note that the pictures (b)–(d) refer to a single geometry parameter x, in practice the same correction-prediction scheme is applied to all relevant geometry parameters simultaneously.

Replace the vector realizing $D_{\max}$ in $\{\boldsymbol{x}^{(j)}\}_{j=1,\ldots,N}$ by $\boldsymbol{x}_{tmp}$;

else

Generate random observables $\boldsymbol{x}_{tmp}$ until satisfying $D(\boldsymbol{F}(\boldsymbol{x}_{tmp}),\boldsymbol{f}_t) < D_{\max}$, in which case the vector realizing $D_{\max}$ in $\{\boldsymbol{x}^{(j)}\}_{j=1,\ldots,N}$ is replaced by $\boldsymbol{x}_{tmp}$; in case of exceeding the computational budget go to 9;

end

8. Update the inverse regression model $r_l(\boldsymbol{F})$ using current set $\{\boldsymbol{x}^{(j)}\}_{j=1,\ldots,N}$;
9. Find $\boldsymbol{x}^{(0)} = \boldsymbol{x}^{(j\min)}$, where $j_{\min} = \operatorname{argmin}\{j = 1,\ldots,N: D(\boldsymbol{F}(\boldsymbol{x}^{(j)}),\boldsymbol{f}_t)\}$;
10. **if** $D(\boldsymbol{F}(x^{(0)}),\boldsymbol{f}_t) \leq D_{accept}$ OR computational budget has been exceeded

Go to 11

else

Go to 6

end

11. Return $\boldsymbol{x}^{(0)}$; END;

The introductory four steps of the procedure describe the initial sampling that leads to identification of N designs featuring clearly-defined characteristics points. These vectors are used to construct the first inverse surrogate r_l (Step 5). In Steps 6 through 10, the inverse model is employed as a predictor tool to yield the candidate design $\boldsymbol{x}_{tmp}$, at which the antenna is intended to have its resonances allocated as close to the target values $\boldsymbol{f}_t$ as possible. The candidate design – provided it is of sufficient quality – replaces the worst observable vector, which is followed by rebuilding the inverse model. The process continues until a sufficiently good design $\boldsymbol{x}^{(0)}$ has been found (i.e., such that $D(\boldsymbol{F}(\boldsymbol{x}^{(0)})\boldsymbol{f}_t) \leq D_{accept}$) or the computational budget is exceeded (in which case the best design found so far is returned as $\boldsymbol{x}^{(0)}$). The design $\boldsymbol{x}^{(0)}$ will undergo local tuning, as described in Section 2.4.

2.4. Local refinement by trust-region gradient search

The acceptance threshold D_{accept} of Section 2.3 is set to ensure that the operating frequencies of the design satisfying the condition $D(\boldsymbol{F}(\boldsymbol{x}^{(0)}),\boldsymbol{f}_t) \le D_{accept}$ are sufficiently close to $\boldsymbol{f}_t$ so that the target values are attainable from $\boldsymbol{x}^{(0)}$ through local search. In this work, we use trust-region (TR) gradient-based optimizer with numerical derivatives as the optimization engine [82]. The TR procedure yields a series of approximations to $\boldsymbol{x}^*$, denoted as $\boldsymbol{x}^{(i)}$, $i = 0, 1, \ldots$, by solving

$$\boldsymbol{x}^{(i+1)} = \arg\min_{\boldsymbol{x};\, -\boldsymbol{d}^{(i)} \le \boldsymbol{x}-\boldsymbol{x}^{(i)} \le \boldsymbol{d}^{(i)}} U_L(\boldsymbol{x},\boldsymbol{f}_t) \tag{6}$$

where U_L is the objective function of the same form as the original function U (cf. (1)), but obtained using the first-order Taylor expansion model $\boldsymbol{G}^{(i)}(\boldsymbol{x},f)$ of antenna responses (rather than directly from EM-simulated responses $S_{11}(\boldsymbol{x},f)$). The linear model is defined as

$$\boldsymbol{G}^{(i)}(\boldsymbol{x},f) = S_{11}(\boldsymbol{x}^{(i)},f) + \nabla_S(\boldsymbol{x}^{(i)},f)\cdot(\boldsymbol{x}-\boldsymbol{x}^{(i)}) \tag{7}$$

with the gradients estimated using finite differentiation. Note that the sub-problem (6) is solved within the interval $\boldsymbol{x}^{(i)} - \boldsymbol{d}^{(i)} \le \boldsymbol{x} \le \boldsymbol{x}^{(i)} + \boldsymbol{d}^{(i)}$, referred to as the trust region (here, the inequalities are understood component wise). The size vector $\boldsymbol{d}^{(i)}$ is adjusted using the standard rules [82]. If the iteration is successful, i.e., $U(\boldsymbol{x}^{(i+1)},\boldsymbol{f}_t) < U(\boldsymbol{x}^{(i)},\boldsymbol{f}_t)$, the design yielded by (6) is accepted and the next iteration begins. The computational cost of updating the linear model is $n + 1$ EM antenna simulation.

The termination condition is convergence in argument $\|\boldsymbol{x}^{(i+1)} - \boldsymbol{x}^{(i)}\| < \varepsilon$, or shrinking the trust region $\|\boldsymbol{d}^{(i)}\| < \varepsilon$ (whichever occurs first). Here, we assume $\varepsilon = 10^{-3}$. The local tuning can be sped up by means of sparse sensitivity updates (e.g., [32,80]). In this work, a very simple mechanism is employed, where the finite differentiation is replaced by the Broyden updating formula [83] when the optimization process is sufficiently close to convergence, or $\|\boldsymbol{x}^{(i+1)} - \boldsymbol{x}^{(i)}\| < 10\varepsilon$.

2.5. Optimization framework

This section briefly summarizes the entire optimization framework proposed in this work. The two major stages thereof are the global search process of Section 2.3, and local refinement of Section 2.4. The control parameters of the algorithm are juxtaposed again below for the convenience of the reader:

- N – the number of observables for inverse model construction;
- $N_{max.1}$ – computational budget: maximum number of EM antenna evaluations for initial sampling;
- $N_{max.2}$ – computational budget: maximum number of EM antenna evaluations for global search stage;
- $N_{max.3}$ – computational budget: maximum number of EM antenna evaluations for local tuning stage;
- D_{accept} – the threshold for accepting designs produced by the global search stage (cf. Section 2.3);
- ε - termination threshold (for convergence in argument and trust-region size, cf. Section 2.4);

It should be noted that the algorithm only has two important control parameters, which are N and D_{accept}. The remaining parameters are standard. In particular, the termination threshold is set to determine the required resolution of the optimization process, whereas the computational budget numbers are typically set up with some margin (in practice, the termination of both global and local search stages is due to convergence rather than exceeding the budget). Now, the number N of samples for inverse model construction is normally kept small, say 10 or 20, which is because the inverse model is set up over low-dimensional operating frequency space, and the number of model coefficients is also low (specifically, $K + 2$). Selection of D_{accept} is somehow problem dependent: in order to ensure that the target frequencies are attainable from $\boldsymbol{x}^{(0)}$ using local search D_{accept} should be set so that the distances between the target frequencies and the actual ones at the initial design are not larger the corresponding impedance bandwidths.

The operating flow of the entire algorithm can be described as follows:

1. Input arguments:
   - Target operating frequencies $\boldsymbol{f}_t$,
   - Objective function U,
   - Parameter space X;
2. Produce initial design $\boldsymbol{x}^{(0)}$ by performing global search (Section 2.3);
3. Obtain final design $\boldsymbol{x}^*$ through local tuning (Section 2.4), using $\boldsymbol{x}^{(0)}$ as the starting point.

Fig. 4 shows the flow diagram of the process. Therein, the global search part has been broken down into several steps, according to the description provided in Section 2.3. The local tuning is represented as a single block.

At this point, it should also be emphasized that the presented approach is not limited to optimization of multi-band antennas in the sense of the objective function (2), i.e., matching improvement at the centre frequencies. It can also be employed to improve matching over the bandwidths centred at the target frequencies, or even bandwidth enhancement. Both would require a different definition of the objective function at the local tuning stage; however, the global search part would remain essentially intact. More detailed treatment of this subject will be provided elsewhere.

3. Demonstration case studies

This section provides numerical verification of the knowledge-based optimization framework proposed in Section 2. The primary novelties of our approach include conceptual development of the decision-making process that identifies the most promising regions of the parameter space, and implementation of the global optimization algorithm for the design of multi-band antennas using feature-based inverse surrogates, as well as low-cost rendition of high-quality initial designs using system-specific knowledge. The numerical verification carried out using three microstrip antennas, a dual-band dipole, and two triple-band structures. The results obtained with our methodology are benchmarked against multiple-start local optimization as well as a representative nature-inspired algorithm (here, the particle swarm optimizer). The proposed framework is demonstrated to be superior over the local optimizer and nature-inspired procedure, as it solves global optimization problems at a cost comparable to that of local search. The major factors considered in the analysis include reliability of the optimization process, quality of the final design, as well as the computational cost.

The remaining part of this part of the paper is organized as follows. Section 3.1 introduces the test antenna geometries and formulates the design tasks. Experimental setup is explained in Section 3.2 along with the numerical results obtained using the proposed and the benchmark techniques. Result discussion is provided in Section 3.3.

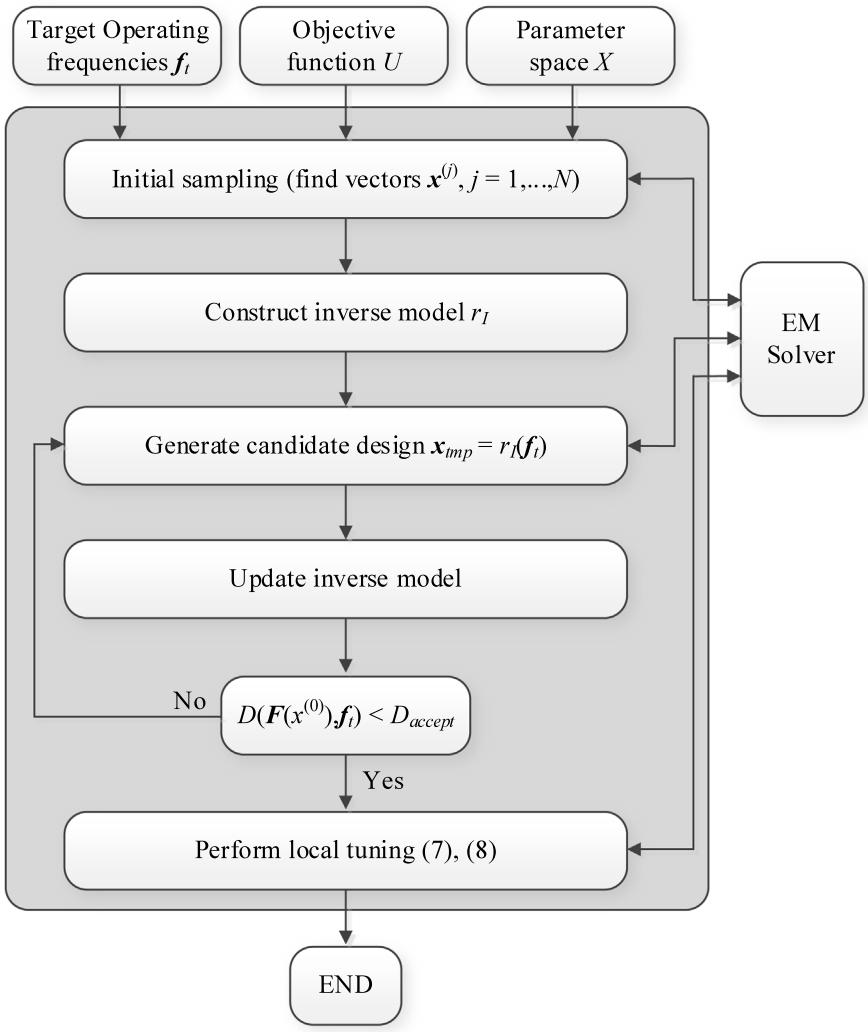

Fig. 4. Flow diagram of the proposed framework for globalized optimization of multi-band antennas.

3.1. Test antenna structures

Fig. 5 shows the three antenna structures employed to validate the globalized optimization framework proposed in this work. These are:

- Antenna I: dual-band uniplanar dipole antenna [84], implemented on RO4350 substrate (ε_r = 3.48, $h = 0.762$ mm). The independent geometry parameters are $\boldsymbol{x} = [l_1 \quad l_2 \quad l_{3r} \quad w_1 \quad w_2 \quad w_3]^T$, with $l_3 = l_{3r}l_1$; we also have $l_0 = 30$, $w_0 = 3$, $s_0 = 0.15$ and $o = 5$; all dimensions except l_{3r} (which is relative) are in mm.
- Antenna II: triple-band dipole antenna [85], also implemented on RO4350 substrate (ε_r = 3.48, $h = 0.762$ mm). The independent geometry parameters are $\boldsymbol{x} = [l_1 \quad l_2 \quad l_{3r} \quad l_4 \quad l_{5r} \quad w_1 \quad w_2 \quad w_3 \quad w_4 \quad w_5]^T$, with $l_3 = l_{3r}l_1$ and $l_5 = l_{5r}l_3$; dimensions $l_0 = 30$, $w_0 = 3$, $s_0 = 0.15$ and $o = 5$ are fixed; dimensions are in mm except l_{3r} and l_{5r}, which are relative.
- Antenna III: triple band U-slotted patch with L-slot DGS [86], implemented on 3.064-mm-thick substrate of relative permittivity 3.2. The independent geometry parameters are $\boldsymbol{x} = [L_1 \quad L_s \quad L_{ur} \quad W \quad W_1 \quad dL_r \quad dW_r \quad g \quad l_{s1r} \quad l_{s2r} \quad w_{ur}]^T$; the following dimensions are fixed: $b = 1$, $w_f = 7.4$, $s = 0.5$, $w = 0.5$, $dL_2 = L_1$; we also have additional relationships: $L = L_s + g + L_1 + dL_2$, $L_u = L_{ur}W_1$, $dL = dL_rL$, $dW = dW_rW$, $l_{s1} = l_{s1r}(L - dL)$, $l_{s2} = l_{s2r}(W - dW)$, $w_u = w_{ur}(L_1 - b - s)$.

The computational models for all structures are implemented in CST Microwave Studio, and simulated using its time-domain solver.

The design tasks are formulated as in Section 2.1 with the objective function in the form of (2). The target frequencies and parameter spaces for Antennas I through III have been listed in Table 1. It should be noticed that the parameter space dimensionalities are relatively large, especially for Antennas II and III, whereas the parameter ranges are very broad: the average upper-to-lower bound ratio is as high as 4.2 for Antenna I, 8.4 for Antenna II, and 2.6 for Antenna III.

3.2. Experimental setup and results

For each test antenna, the optimization process is executed ten times using the following algorithms:

- The proposed inverse-surrogate-based framework of Section 2. The control parameters are set as follows (the same for all cases): $N = 10$, $N_{\max.1} = 100$, $N_{\max.2} = 100$, $N_{\max.3} = 500$, $\varepsilon = 10^{-3}$, $D_{accept} = 0.2$;

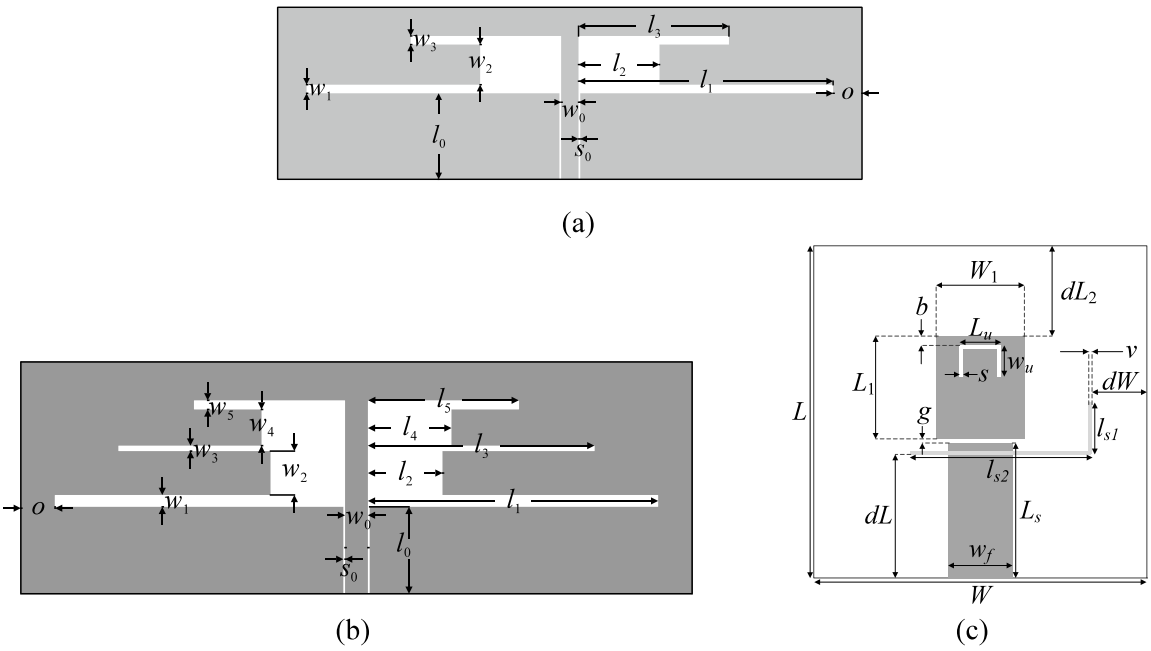

Fig. 5. Verification antenna structures: (a) Antenna I [84], (b) Antenna II [85], (c) Antenna III [86], the light-shade grey denotes a ground-plane slot.

Table 1
Target operating frequencies and parameter spaces for Antennas I through III.

Antenna	Target operating frequencies [GHz]	Parameter space X (lower bounds $\boldsymbol{l}$ and upper bounds $\boldsymbol{u}$)
I	$\boldsymbol{f}_t = [2.45\ 5.3]^T$	$\boldsymbol{l} = [15\ 3\ 0.35\ 0.2\ 1.8\ 0.5]^T$ $\boldsymbol{u} = [50\ 12\ 0.85\ 1.5\ 4.3\ 2.7]^T$
II	$\boldsymbol{f}_t = [2.45\ 3.6\ 5.3]^T$	$\boldsymbol{l} = [20\ 3\ 0.6\ 3\ 0.6\ 0.2\ 0.2\ 0.2\ 0.2\ 0.2]^T$ $\boldsymbol{u} = [50\ 5\ 0.85\ 5\ 0.85\ 2.2\ 4.2\ 2.2\ 4.2\ 2.2]^T$
III	$\boldsymbol{f}_t = [3.5\ 5.8\ 7.5]^T$	$\boldsymbol{l} = [10\ 17\ 0.2\ 45\ 5\ 0.4\ 0.15\ 0.2\ 0.1\ 0.5\ 0.1]^T$ $\boldsymbol{u} = [16\ 25\ 0.6\ 55\ 15\ 0.5\ 0.3\ 0.8\ 0.4\ 0.65\ 0.5]^T$

- Particle swarm optimizer (PSO) [87] using the swarm size of 10, with maximum number of iterations 50 (Version I) and 100 (Version II), and the standard control parameter setup ($\chi = 0.73$, $c_1 = c_2 = 2.05$);
- Trust-region gradient-based optimization using the algorithm of Section 2.4; each run is executed using a random starting point.

PSO is employed as a representative nature-inspired global optimization routine, whereas local optimization is included in order to demonstrate the need for global optimization for the considered test problems.

The optimization results have been gathered in Tables 2 through 4. Figs. 6–8 show – for the selected algorithm runs – the antenna responses at the final designs obtained using the proposed framework, for Antennas I, II, and III, respectively.

3.3. Discussion

The results provided in Tables 2 through 4 demonstrate truly global optimization capabilities of the inverse-modelling-based procedure proposed in this work. In the analysis below we focus on the three aspects of the optimization process:

- *Reliability*: The proposed algorithm consistently finds satisfactory design (i.e., appropriately allocates the antenna operating frequencies) at all of its runs and for all considered antenna structures. A comparison with local search indicates that the design task is indeed multimodal and inadequate choice of the initial design results in poor performance (satisfactory designs found in less than 50 percent of the cases on the average). Reliability of PSO is noticeably better, although it is not as good as for the proposed approach. Also, restricting the computational budget to 500 antenna simulations has a detrimental effect on the reliability, which suggests that 1,000 objective function calls is about a minimum number required to maintain practical result repeatability.
- *Design quality*: The proposed algorithm clearly ensures the best design quality as measured by the average objective function value. It is considerably better than both the local routine and PSO (in both 50 and 100 iteration versions).
- *Computational cost*: The computational efficiency of the proposed method is considerably better than PSO. What is more important, the average cost of our procedure is comparable to that of the gradient search. The average expenses are only about 45 percent higher, which is negligible having in mind that this small extra cost enables global search capabilities. It should also be mentioned that the average cost of the global search stage for the proposed algorithm is 34, 40, and 36 antenna simulations for Antennas I, II, and III, respectively, which is about 25 percent of the overall costs. This indicates that a combination of response features and inverse surrogates constitutes a quite powerful tool that allows us to exploit the dependence between the antenna operating frequencies and its geometry parameters at minimum computational budget. Whereas the number of iterations of the local search are equal to 17, 12 and 9 for the respective antennas. The remaining details on the optimization task are the following. The imposed constraints include only lower and upper bounds on the geometry parameters,

Table 2
Optimization results for Antenna I.

Optimization method	Inverse-surrogate-based algorithm (this work)	PSO		Trust-region gradient-based algorithm
		50 iterations	100 iterations	
Average objective function value [dB]	−26.4	−18.2	−19.3	−13.5
Computational cost[a]	144.7	500	1,000	84.2
Success rate[b]	10/10	9/10	10/10	6/10

[a]The cost expressed in terms of the number of EM simulations of the antenna structure under design.
[b]Number of algorithms runs at which the operating frequencies were allocated with sufficient accuracy, i.e., to satisfy the condition $D(\boldsymbol{F}(\boldsymbol{x}^*),\boldsymbol{f}_t) \leq D_{accept}$.

Table 3
Optimization results for Antenna II.

Optimization method	Inverse-surrogate-based algorithm (this work)	PSO		Trust-region gradient-based algorithm
		50 iterations	100 iterations	
Average objective function value [dB]	−17.9	−10.8	−13.8	−7.8
Computational cost[a]	171.1	500	1,000	105.8
Success rate[b]	10/10	5/10	8/10	4/10

[a]The cost expressed in terms of the number of EM simulations of the antenna structure under design.
[b]Number of algorithms runs at which the operating frequencies were allocated with sufficient accuracy, i.e., to satisfy the condition $D(\boldsymbol{F}(\boldsymbol{x}^*),\boldsymbol{f}_t) \leq D_{accept}$.

Table 4
Optimization results for Antenna III.

Optimization method	Inverse-surrogate-based algorithm (this work)	PSO		Trust-region gradient-based algorithm
		50 iterations	100 iterations	
Average objective function value [dB]	−20.2	−12.3	−14.2	−12.1
Computational cost[a]	142.6	500	1,000	125.4
Success rate[b]	10/10	6/10	8/10	4/10

[a]The cost expressed in terms of the number of EM simulations of the antenna structure under design.
[b]Number of algorithms runs at which the operating frequencies were allocated with sufficient accuracy, i.e., to satisfy the condition $D(\boldsymbol{F}(\boldsymbol{x}^*),\boldsymbol{f}_t) \leq D_{accept}$.

and the algorithm is set up to preserve feasibility of solutions, which is simply achieved by imposing box-constraints when optimizing linear model of the trust-region algorithm. It should also be observed, that the optimization task is formulated in a minimax sense, and the optimum is not known beforehand (i.e., there is no target solution the algorithm is aiming at).

The aforementioned features of the introduced optimization procedure make it a potentially useful tool for handling global optimization tasks for multi-band antennas. The repeatability of solutions produced by the procedure is remarkable while maintaining the computational efficiency comparable to that of gradient-based local optimizers.

The proposed procedure can be employed for solving optimization tasks, especially in the cases when the objective function is expensive to calculate. The sole limitation is that the antenna structure under design featured suitably shaped responses with easily distinguishable characteristic points. The proposed procedure may be generalized to other types of antenna characteristics, as well as applied to other classes of high-frequency components.

4. Conclusion

The paper proposed a novel algorithm for globalized optimization of multi-band antennas. Our approach involves an inverse regression model established using a set of random observables, and employed to determine the relationships between the antenna target operating frequencies and geometry parameters. Its construction relies on response feature technology to avoid direct processing of complete frequency characteristics and to capitalize on slightly nonlinear dependence of the feature point coordinates and antenna dimensions. Owing to the exploitation of the system-specific knowledge, the proposed framework is both reliable and sufficient: the knowledge-based inverse surrogate employed in the decision-making process yields a high-quality initial design that only needs to be locally tuned to render optimal design satisfying the assumed design specifications. The presented methodology has been validated with the use of three microstrip antennas, and demonstrated to properly allocate the operating frequencies for all algorithm runs. Benchmarking against multiple-start local search as well as nature-inspired metaheuristic procedures (here, particle swarm optimization) indicate superior efficacy of the proposed procedure both in terms of reliability and computational costs. More specifically, the typical cost of the optimization process is comparable to that of local gradient-based tuning, and, at the same time, it is significantly lower than for population-based routines. The presented approach can be considered a viable alternative to existing methodologies, especially in terms of ensuring global search capabilities at low computational expenses. It should be observed that the applicability of our method is limited to antenna structures of suitably shaped responses featuring easily distinguishable characteristic points. Still, the characteristics of different types of real-world antennas are, as a matter of fact, appropriately structured (e.g., multi-band antennas employed here as verification case studies). The future work will be focused on generalization of the method to other types of antenna characteristics, as well as applications to other classes of high-frequency components.

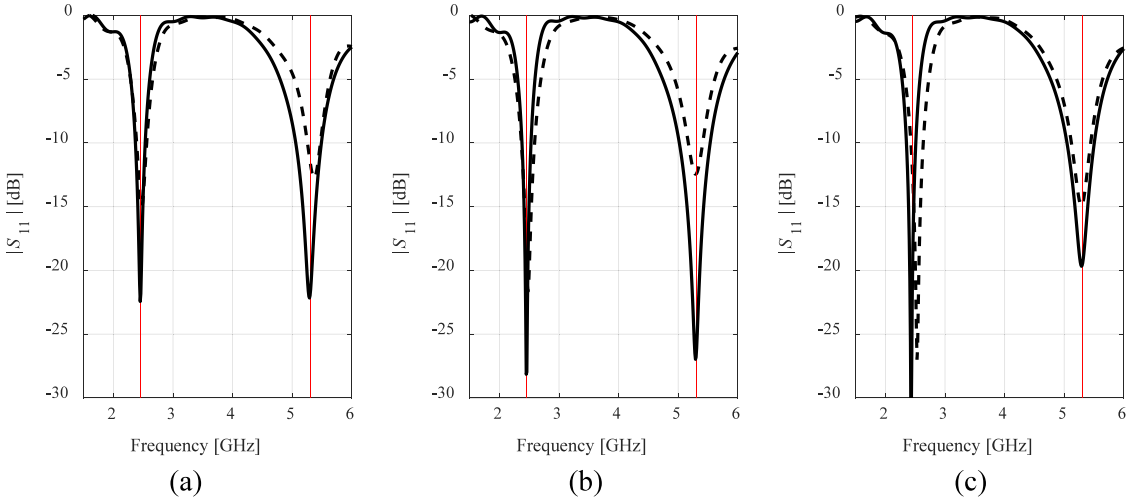

Fig. 6. Antenna I responses at the designs obtained using the proposed global optimization framework for selected algorithm runs: (a) run 1, (b) run 2, (c) run 3. Dashed line shows the initial design $\boldsymbol{x}^{(0)}$ obtained after the global search stage, solid line represents the antenna response at the final design. Vertical lines mark the target operating frequencies, here 2.45 GHz and 5.3 GHz.

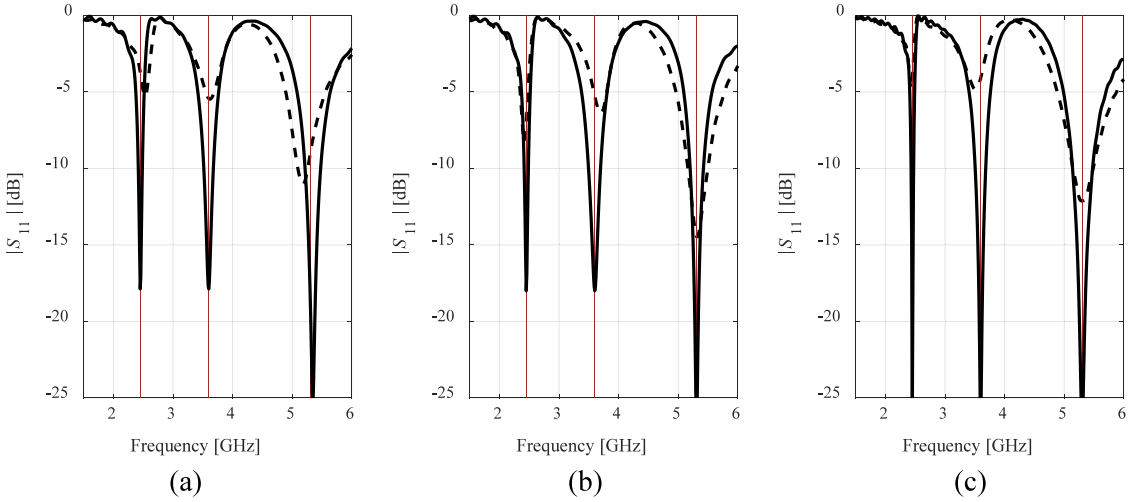

Fig. 7. Antenna II responses at the designs obtained using the proposed global optimization framework for selected algorithm runs: (a) run 1, (b) run 2, (c) run 3. Dashed line shows the initial design $\boldsymbol{x}^{(0)}$ obtained after the global search stage, solid line represents the antenna response at the final design. Vertical lines mark the target operating frequencies, here 2.45 GHz, 3.6 GHz, and 5.3 GHz.

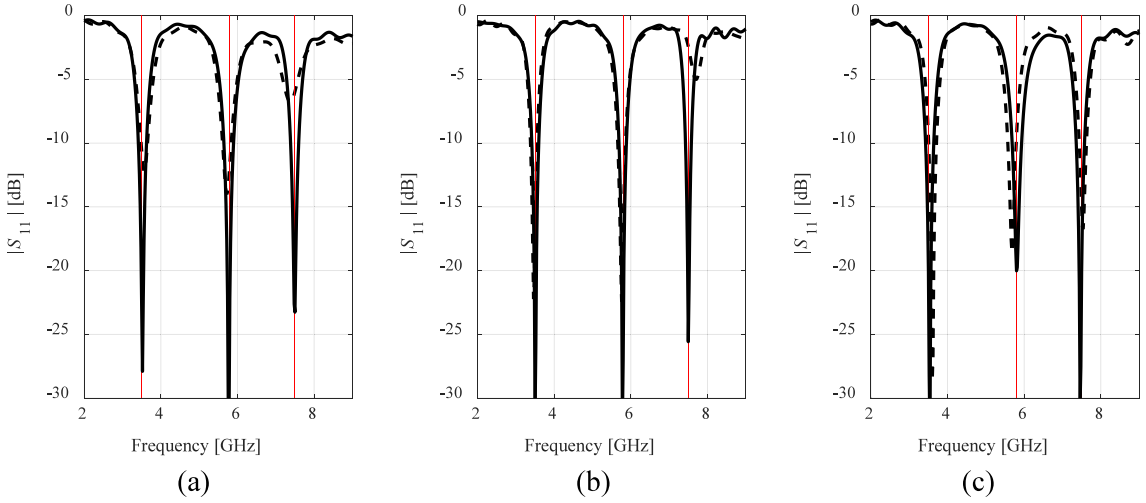

Fig. 8. Antenna III responses at the designs obtained using the proposed global optimization framework for selected algorithm runs: (a) run 1, (b) run 2, (c) run 3. Dashed line shows the initial design $\boldsymbol{x}^{(0)}$ obtained after the global search stage, solid line represents the antenna response at the final design. Vertical lines mark the target operating frequencies, here 3.5 GHz, 5.8 GHz, and 7.5 GHz.

CRediT authorship contribution statement

Slawomir Koziel: Conceptualization, Formal analysis, Funding acquisition, Methodology, Project administration, Resources, Software, Supervision, Validation, Visualization, Writing - original draft, Writing - review & editing. **Anna Pietrenko-Dabrowska:** Conceptualization, Data curation, Investigation, Methodology, Software, Validation, Visualization, Writing - original draft, Writing - review & editing.

Declaration of competing interest

The authors declare that they have no known competing financial interests or personal relationships that could have appeared to influence the work reported in this paper.

Acknowledgements

The authors would like to thank Dassault Systemes, France, for making CST Microwave Studio available. This work is partially supported by the Icelandic Centre for Research (RANNIS) Grant 217771 and by National Science Centre of Poland Grant 2020/37/B/ST7/01448.

References

[1] S. Wen, Y. Dong, A low-profile wideband antenna with monopolelike radiation characteristics for 4G/5g indoor micro base station application, IEEE Ant. Wirel. Prop. Lett. 19 (12) (2020) 2305–2309.
[2] Y. Zhang, J. Deng, M. Li, D. Sun, L. Guo, A MIMO dielectric resonator antenna with improved isolation for 5G mm-wave applications, IEEE Ant. Wirel. Prop. Lett. 18 (4) (2019) 747–751.
[3] Z. Fu, F. Yang, A slotted patch antenna integrated with thermal switch for high-sensitivity temperature monitoring, IEEE Ant. Wirel. Prop. Lett. 14 (2015) 998–1001.
[4] X. Lin, Y. Chen, Z. Gong, B. Seet, L. Huang, Y. Lu, Ultrawideband textile antenna for wearable microwave medical imaging applications, IEEE Trans. Ant. Prop. 68 (6) (2020) 4238–4249.
[5] K.R. Jha, B. Bukhari, C. Singh, G. Mishra, S.K. Sharma, Compact planar multistandard MIMO antenna for IoT applications, IEEE Trans. Ant. Prop. 66 (7) (2018) 3327–3336.
[6] L. Sun, Y. Li, Z. Zhang, Z. Feng, Wideband 5G MIMO antenna with integrated orthogonal-mode dual-antenna pairs for metal-rimmed smartphones, IEEE Trans. Ant. Prop. 68 (4) (2020) 2494–2503.
[7] C.G. Hynes, R.G. Vaughan, Conical monopole antenna with integrated tunable notch filters, IEEE Ant. Wirel. Prop. Lett. 19 (12) (2020) 2398–2402.
[8] J. Liu, Z. Tang, Z. Wang, H. Li, Y. Yin, Gain enhancement of a broadband symmetrical dual-loop antenna using shorting pins, IEEE Ant. Wirel. Prop. Lett. 17 (8) (2018) 1369–1372.
[9] Y. Dong, J. Choi, T. Itoh, Vivaldi antenna with pattern diversity for 0.7 to 2.7 GHz cellular band applications, IEEE Ant. Wirel. Prop. Lett. 17 (2) (2018) 247–250.
[10] A. Zhao, Z. Ren, Size reduction of self-isolated MIMO antenna system for 5G mobile phone applications, IEEE Ant. Wirel. Prop. Lett. 18 (1) (2019) 152–156.
[11] G. Gao, C. Yang, B. Hu, R. Zhang, S. Wang, A wearable PIFA with an all-textile metasurface for 5 GHz WBAN applications, IEEE Ant. Wirel. Prop. Lett. 18 (2) (2019) 288–292.
[12] L. Xu, J. Xu, Z. Chu, S. Liu, X. Zhu, Circularly polarized implantable antenna with improved impedance matching, IEEE Ant. Wirel. Prop. Lett. 19 (5) (2020) 876–880.
[13] S.K. Podilchak, J.C. Johnstone, M. Caillet, M. Clénet, Y.M.M. Antar, A compact wideband dielectric resonator antenna with a meandered slot ring and cavity backing, IEEE Ant. Wirel. Prop. Lett. 15 (2016) 909–913.
[14] W. Hu, Y. Yin, X. Yang, P. Fei, Compact multiresonator-loaded planar antenna for multiband operation, IEEE Trans. Ant. Prop. 61 (5) (2013) 2838–2841.
[15] S. Zhu, H. Liu, P. Wen, Z. Chen, H. Xu, Vivaldi antenna array using defected ground structure for edge effect restraint and back radiation suppression, IEEE Ant. Wirel. Prop. Lett. 19 (1) (2020) 84–88.
[16] Z. Ding, R. Jin, J. Geng, W. Zhu, X. Liang, Varactor loaded pattern reconfigurable patch antenna with shorting pins, IEEE Trans. Ant. Prop. 67 (10) (2019) 6267–6277.
[17] M. Mosalanejad, I. Ocket, C. Soens, G.A.E. Vandenbosch, Multi-layer PCB bow-tie antenna array for (77–81) GHz radar applications, IEEE Trans. Ant. Prop. 68 (3) (2020) 2379–2386.
[18] R. Sayyadi, A. Awasthi, A simulation-based optimisation approach for identifying key determinants for sustainable transportation planning, Int. J. Syst. Sci.: Oper. Logist. 5 (2) (2018) 161–174.
[19] A. Gharaei, S.A.H. Shekarabi, M. Karimi, Modelling and optimal lot-sizing of the replenishments in constrained, multi-product and bi-objective EPQ models with defective products: Generalised cross decomposition, Int. J. Syst. Sci.: Oper. Logist. 7 (3) (2020) 262–274.
[20] Y.-C. Tsao, Design of a carbon-efficient supply-chain network under trade credits, Int. J. Syst. Sci.: Oper. Logist. 2 (3) (2015) 177–186.
[21] A. Gharaei, M. Karimi, S.A.H. Shekarabi, Joint economic lot-sizing in multi-product multi-level integrated supply chains: Generalized benders decomposition, Int. J. Syst. Sci.: Oper. Logist. 7 (4) (2020) 309–325.
[22] S.A.H. Shekarabi, A. Gharaei, M. Karimi, Modelling and optimal lot-sizing of integrated multi-level multi-wholesaler supply chains under the shortage and limited warehouse space: Generalised outer approximation, Int. J. Syst. Sci.: Oper. Logist. 6 (3) (2019) 237–257.
[23] C. Duan, C. Deng, A. Gharaei, J. Wu, B. Wang, Selective maintenance scheduling under stochastic maintenance quality with multiple maintenance actions, In. J. Prod. Res. 56 (23) (2018) 7160–7178.
[24] A. Gharaei, S.A.H. Shekarabi, M. Karimi, E. Pourjavad, A. Amjadian, An integrated stochastic EPQ model under quality and green policies: Generalised cross decomposition under the separability approach, Int. J. Syst. Sci.: Oper. Logist. (2019).
[25] S. Liang, Z. Fang, G. Sun, Y. Liu, G. Qu, Y. Zhang, Sidelobe reductions of antenna arrays via an improved chicken swarm optimization approach, IEEE Access 8 (2020) 37664–37683.
[26] M. Tang, X. Chen, M. Li, R.W. Ziolkowski, Particle swarm optimized, 3-D-printed, wideband, compact hemispherical antenna, IEEE Ant. Wirel. Prop. Lett. 17 (11) (2018) 2031–2035.
[27] S. Genovesi, R. Mittra, A. Monorchio, G. Manara, Particle swarm optimization for the design of frequency selective surfaces, IEEE Ant. Wirel. Prop. Lett. 5 (2006) 277–279.
[28] W. Li, Y. Zhang, X. Shi, Advanced fruit fly optimization algorithm and its application to irregular subarray phased array antenna synthesis, IEEE Access 7 (2019) 165583–165596.
[29] Z.J. Jiang, S. Zhao, Y. Chen, T.J. Cui, Beamforming optimization for time-modulated circular-aperture grid array with DE algorithm, IEEE Ant. Wirel. Prop. Lett. 17 (12) (2018) 2434–2438.
[30] J.A. Tomasson, S. Koziel, A. Pietrenko-Dabrowska, Quasi-global optimization of antenna structures using principal components and affine subspace-spanned surrogates, IEEE Access 8 (2020) 50078–50084.
[31] J.A. Tomasson, A. Pietrenko-Dabrowska, S. Koziel, Expedited globalized antenna optimization by principal components and variable-fidelity EM simulations: application to microstrip antenna design, Electronics 9 (4) (2020).
[32] S. Koziel, A. Pietrenko-Dabrowska, Expedited feature-based quasi-global optimization of multi-band antennas with Jacobian variability tracking, IEEE Access 8 (2020) 83907–83915.
[33] L.M.Q. Abualigah, Feature Selection and Enhanced Krill Herd Algorithm for Text Document Clustering, Springer, 2019.
[34] L. Abualigah, A. Diabat, S. Mirjalili, M.A. Elaziz, A.H. Gandomi, The arithmetic optimization algorithm, Comp. Methods Applied Mech. Eng. 376 (2021) 113609.
[35] L. Abualigah, D. Yousri, M.A. Elaziz, A.A. Ewees, M.A.A. Al-qaness, A.H. Gandomi, Aquila optimizer: A novel meta-heuristic optimization algorithm, Comp. Industr. Eng. (2021) 107250.
[36] L. Abualigah, A. Diabat, Advances in sine cosine algorithm: A comprehensive survey, Art. Intell. Rev. 54 (2021) 2567–2608.
[37] A. Darvish, A. Ebrahimzadeh, Improved fruit-fly optimization algorithm and its applications in antenna arrays synthesis, IEEE Trans. Ant. Prop. 66 (4) (2018) 1756–1766.
[38] Z. Bayraktar, M. Komurcu, J.A. Bossard, D.H. Werner, The wind driven optimization technique and its application in electromagnetics, IEEE Trans. Ant. Prop. 61 (5) (2013) 2745–2757.
[39] A.A. Al-Azza, A.A. Al-Jodah, F.J. Harackiewicz, Spider monkey optimization: a novel technique for antenna optimization, IEEE Ant. Wirel. Prop. Lett. 15 (2016) 1016–1019.
[40] J.M. Kovitz, Y. Rahmat-Samii, Ensuring robust antenna designsusing multiple diverse optimization techniques, in: Proc. IEEE Ant. Propag. Symp. 2013, pp. 408–409.
[41] M. Kovaleva, D. Bulger, K.P. Esselle, Comparative study of optimization algorithms on the design of broadband antennas, IEEE J. Multis. Multiph. Comp. Techn. 5 (2020) 89–98.
[42] T.C. Bora, L. Lebensztajn, L.D.S. Coelho, Non-dominated sorting genetic algorithm based on reinforcement learning to optimization of broad-band reflector antennas satellite, IEEE Trans. Magn. 48 (2) (2012) 767–770.

[43] D. Ding, G. Wang, Modified multiobjective evolutionary algorithm based on decomposition for antenna design, IEEE Trans. Ant. Prop. 61 (10) (2013) 5301–5307.
[44] D.Z. Zhu, P.L. Werner, D.H. Werner, Design and optimization of 3-D frequency-selective surfaces based on a multiobjective lazy ant colony optimization algorithm, IEEE Trans. Ant. Prop. 65 (12) (2017) 7137–7149.
[45] K. Choi, D. Jang, S. Kang, J. Lee, T. Chung, H. Kim, Hybrid algorithm combing genetic algorithm with evolution strategy for antenna design, IEEE Trans. Magn. 52 (3) (2016) 7209004.
[46] L.A. Greda, A. Winterstein, D.L. Lemes, M.V.T. Heckler, Beamsteering and beamshaping using a linear antenna array based on particle swarm optimization, IEEE Access 7 (2019) 141562–141573.
[47] C. Cui, Y. Jiao, L. Zhang, Synthesis of some low sidelobe linear arrays using hybrid differential evolution algorithm integrated with convex programming, IEEE Ant. Wirel. Prop. Lett. 16 (2017) 2444–2448.
[48] P. Baumgartner, T. Baurnfeind, O. Biro, A. Hackl, C. Magele, W. Renhart, R. Torchio, Multi-objective optimization of Yagi-Uda antenna applying enhanced firefly algorithm with adaptive cost function, IEEE Trans. Magn. 54 (3) (2018) 8000504.
[49] S.H. Yang, J.F. Kiang, Optimization of sparse linear arrays using harmony search algorithms, IEEE Trans. Ant. Prop. 63 (11) (2015) 4732–4738.
[50] X. Li, K.M. Luk, The grey wolf optimizer and its applications in electromagnetics, IEEE Trans. Ant. Prop. 68 (3) (2020) 2186–2197.
[51] G. Ram, D. Mandal, R. Kar, S.P. Ghoshal, Cat swarm optimization as applied to time-modulated concentric circular antenna array: analysis and comparison with other stochastic optimization methods, IEEE Trans. Ant. Prop. 63 (9) (2015) 4180–4183.
[52] S.K. Goudosetal, Novel spiral antenna design using artificial bee colony optimization for UHF RFID applications, IEEE Ant. Wirel. Prop. Lett. 13 (2014) 528–531.
[53] S. Karimkashi, A.A. Kishk, Invasive weed optimization and its features in electromagnetics, IEEE Trans. Ant. Prop. 58 (4) (2010) 1269–1278.
[54] D. Simon, Evolutionary Optimization Algorithms, John Wiley & Sons, Inc. Hoboken, New Jersey, 2013.
[55] A. Lalbakhsh, M.U. Afzal, K.P. Esselle, Multiobjective particle swarm optimization to design a time-delay equalizer metasurface for an electromagnetic band-gap resonator antenna, IEEE Ant. Wirel. Prop. Lett. 16 (2017) 912–915.
[56] X. Jia, G. Lu, A hybrid taguchi binary particle swarm optimization for antenna designs, IEEE Ant. Wirel. Prop. Lett. 18 (8) (2019) 1581–1585.
[57] T. Zheng, Y. Liu, G. Sun, L. Zhang, S. Lian, A. Wang, X. Zhou, IWORMLF: improved invasive weed optimization with random mutation and Lévy flight for beam pattern optimizations of linear and circular antenna arrays, IEEE Access 8 (2020) 19460–19478.
[58] H. Li, Y. Jiang, Y. Ding, J. Tan, J. Zhou, Low-sidelobe pattern synthesis for sparse conformal arrays based on PSO-SOCP optimization, IEEE Access 6 (2018) 77429–77439.
[59] N.V. Queipo, R.T. Haftka, W. Shyy, T. Goel, R. Vaidynathan, P.K. Tucker, Surrogate-based analysis and optimization, Progr. Aero. Sci. 41 (1) (2005) 1–28.
[60] J.A. Easum, J. Nagar, P.L. Werner, D.H. Werner, Efficient multi-objective antenna optimization with tolerance analysis through the use of surrogate models, IEEE Trans. Ant. Prop. 66 (12) (2018) 6706–6715.
[61] B. Liu, H. Aliakbarian, Z. Ma, G.A.E. Vandenbosch, G. Gielen, P. Excell, An efficient method for antenna design optimization based on evolutionary computation and machine learning techniques, IEEE Trans. Ant. Prop. 62 (1) (2014) 7–18.
[62] D.I.L. de Villiers, I. Couckuyt, T. Dhaene, Multi-objective optimization of reflector antennas using kriging and probability of improvement, in: Int. Symp. Ant. Prop., 2017, pp. 985-986.
[63] J.P. Jacobs, Characterization by Gaussian processes of finite substrate size effects on gain patterns of microstrip antennas, IET Microw. Ant. Prop. 10 (11) (2016) 1189–1195.
[64] J. Dong, W. Qin, M. Wang, Fast multi-objective optimization of multi-parameter antenna structures based on improved BPNN surrogate model, IEEE Access 7 (2019) 77692–77701.
[65] I. Couckuyt, F. Declercq, T. Dhaene, H. Rogier, L. Knockaert, Surrogate-based infill optimization applied to electromagnetic problems, Int. J. RF Micr. CAE. 20 (5) (2010) 492–501.
[66] A.M. Alzahed, S.M. Mikki, Y.M.M. Antar, Nonlinear mutual coupling compensation operator design using a novel electromagnetic machine learning paradigm, IEEE Ant. Wirel. Prop. Lett. 18 (5) (2019) 861–865.
[67] J. Tak, A. Kantemur, Y. Sharma, H. Xin, A 3-D-printed W-band slotted waveguide array antenna optimized using machine learning, IEEE Ant. Wirel. Prop. Lett. 17 (11) (2018) 2008–2012.
[68] H.M. Torun, M. Swaminathan, High-dimensional global optimization method for high-frequency electronic design, IEEE Trans. Microw. Theory Techn. 67 (6) (2019) 2128–2142.
[69] B. Liu, S. Koziel, Q. Zhang, A multi-fidelity surrogate-model-assisted evolutionary algorithm for computationally expensive optimization problems, J. Comp. Sc. 12 (2016) 28–37.
[70] B. Xia, Z. Ren, C.S. Koh, Utilizing kriging surrogate models for multi-objective robust optimization of electromagnetic devices, IEEE Trans. Magn. 50 (2) (2014) 7017104.
[71] N. Taran, D.M. Ionel, D.G. Dorrell, Two-level surrogate-assisted differential evolution multi-objective optimization of electric machines using 3-D FEA, IEEE Trans. Magn. 54 (11) (2018) 8107605.
[72] Z. Lv, L. Wang, Z. Han, J. Zhao, W. Wang, Surrogate-assisted particle swarm optimization algorithm with Pareto active learning for expensive multi-objective optimization, IEEE/CAA J. Autom. Sinica 6 (3) (2019) 838–849.
[73] S. Koziel, Low-cost data-driven surrogate modeling of antenna structures by constrained sampling, IEEE Ant. Wirel. Prop. Lett. 16 (2017) 461–464.
[74] S. Koziel, A.T. Sigurdsson, Triangulation-based constrained surrogate modeling of antennas, IEEE Trans. Ant. Prop. 66 (8) (2018) 4170–4179.
[75] S. Koziel, A. Pietrenko-Dabrowska, Performance-based nested surrogate modeling of antenna input characteristics, IEEE Trans. Ant. Prop. 67 (5) (2019) 2904–2912.
[76] S. Koziel, A. Pietrenko-Dabrowska, Performance-Driven Surrogate Modeling of High-Frequency Structures, Springer, New York, 2020.
[77] A. Pietrenko-Dabrowska, S. Koziel, Antenna modeling using variable-fidelity EM simulations and constrained co-kriging, IEEE Access 8 (1) (2020) 91048–91056.
[78] S. Koziel, A. Pietrenko-Dabrowska, Recent advances in accelerated multi-objective design of high-frequency structures using knowledge-based constrained modeling approach, Knowl.-Based Syst. 214 (2021) 106726.
[79] S. Koziel, Fast simulation-driven antenna design using response-feature surrogates, Int. J. RF Micr. CAE 25 (5) (2015) 394–402.
[80] S. Koziel, A. Pietrenko-Dabrowska, Expedited feature-based quasi-global optimization of multi-band antennas with Jacobian variability tracking, IEEE Access 8 (2020) 83907–83915.
[81] S. Koziel, J.W. Bandler, Reliable microwave modeling by means of variable-fidelity response features, IEEE Trans. Microw. Theory Techn. 63 (12) (2015) 4247–4254.
[82] A.R. Conn, N.I.M. Gould, P.L. Toint, Trust region methods, MPS-SIAM series on optimization, 2000.
[83] S. Koziel, A. Pietrenko-Dabrowska, Expedited optimization of antenna input characteristics with adaptive Broyden updates, Eng. Comp. 37 (3) (2019) 851–862.
[84] Y.-C. Chen, S.-Y. Chen, P. Hsu, Dual-band slot dipole antenna fed by a coplanar waveguide, in: Proc. IEEE Antennas Propag. Soc. Int. Symp., 2006, pp. 3589-3592.
[85] A. Pietrenko-Dabrowska, S. Koziel, Simulation-driven antenna modeling by means of response features and confined domains of reduced dimensionality, IEEE Access 8 (2020) 228942–228954.
[86] P. Consul, Triple band gap coupled microstrip U-slotted patch antenna using L-slot DGS for wireless applications, in: Comm., Control Intelligent Syst. (CCIS), Mathura, India, 2015, pp. 31-34.
[87] J. Kennedy, R.C. Eberhart, Swarm Intelligence, Morgan Kaufmann, San Francisco, USA, 2001.